Biochar

ORIGINAL RESEARCH

Tri-functional lanthanum-based biochar for efficient phosphorus recovery, bacterial inhibition, and soil fertility enhancement

Xiuxiu Jia[1], Xue Zhao[2], Yingtang Zhou[3], Fan Li[4], Wen Liu[4*], Yimin Huang[1], Hucai Zhang[1], Jinxing Ma[5*] and Guangzhi Hu[1*]

Abstract

Excess phosphorus (P) in water can lead to eutrophication and upset ecological balance. In this study, biochar with ultrathin two-dimensional nanosheets from the natural mesocarp of shaddock was chosen as the carrier. The highly dispersed and small particle size of $La(OH)_3$ on the surface of the nanosheets (MSBL3) was successfully achieved using chemical impregnation for the adsorption of P in aqueous solution, and the maximum adsorption capacity was 260.0 mg P g^{-1} [La]. The differences in surface crystallization of $La(OH)_3$ on biochar at different La loadings were analyzed using the high-precision characterization methods. After six adsorption–desorption cycles, MSBL3 retained 76.7% of its initial performance in terms of the P adsorption capacity. The preparation of 1 g of MSBL3 costs about RMB 1, and it could reduce the P concentration in 2.6 ton of *Laoyu River* water to below the eutrophication threshold; and the inhibitory effect of MSBL3 on the eutrophication of water bodies was confirmed by the growth state of water hyacinth. Furthermore, 0.1 M MSBL3 could inhibit *Escherichia coli* and *Staphylococcus aureus* up to 98.7% and 85.0%, respectively, which indicates that MSBL3 can be used to recover P from water and also to improve water quality. In addition, the growth of the maize seedlings verified that the P-absorbed MSBL3 waste is a good soil fertilizer and can solve the problem of post-treatment of the adsorbent. In conclusion, MSBL3 prepared in this study is a promising P sorbent for application.

Highlights

- Ultra-small size $La(OH)_3$ was highly homogeneously dispersed on two-dimensional nanosheets of MSBL3.
- Preparation of shaddock mesocarp biochar (MSBL3) for phosphorus adsorption, enabling the resourcefulness of biomass.
- MSBL3 can be used to recover P from water and improve water quality, and its waste can improve soil fertility.

*Correspondence:
Wen Liu
wen.liu@pku.edu.cn
Jinxing Ma
jinxing.ma@gdut.edu.cn
Guangzhi Hu
guangzhihu@ynu.edu.cn
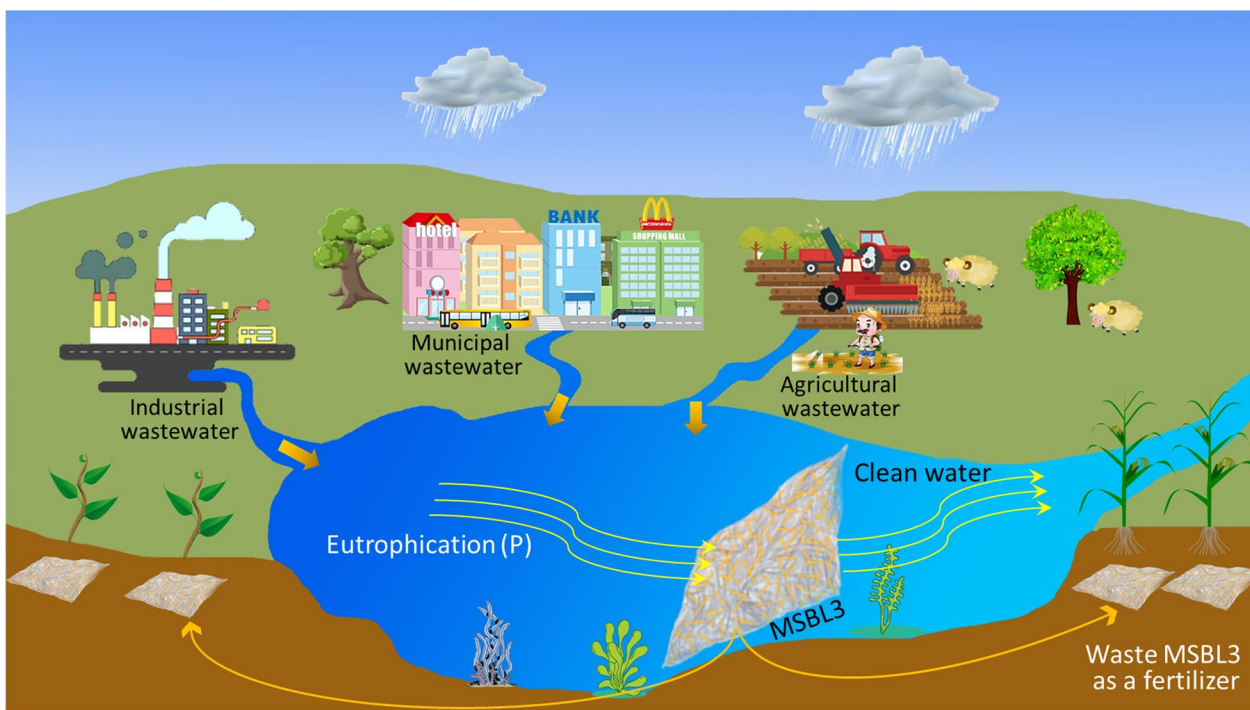Full list of author information is available at the end of the article

Springer

Graphical Abstract

1 Introduction

Phosphorus (P) is closely related to human production and is an essential element in agricultural fertilizers, pesticides, food additives, detergents, and various chemicals (Zhao et al. 2020). The widespread use of P has been accompanied by an increasingly negative impact on the environment, such as causing water eutrophication and ecosystem imbalance, which seriously threatens the health of humans and aquatic animals. Therefore, many regulatory authorities impose strict restrictions on the P content of water. For example, the United States Environmental Protection Agency (USEPA) requires that the total P concentration in water should not be higher than 50 μg L^{-1} and Yao et al. (2013) believes that to prevent water pollution and eutrophication, the total P content should be less than 20 μg L^{-1}. Excess P in aquatic environments is harmful, but paradoxically, there is a global P resource crisis. According to statistics, the human demand for P fertilizer is tens of millions of tons per year (expected to reach 50 million tons by 2023) (Almanassra et al. 2021).

However, current P resources can only meet human needs for a certain number of years (Cordell et al. 2011). If excess P in water bodies can be recovered and reused effectively, the P resource crisis can be alleviated to some extent (He et al. 2022).

Common methods developed to remove P species from aquatic environments include chemical precipitation (Barca et al. 2012), microbial transformation (Geng et al. 2018), enhanced biological phosphorus removal (EBPR), and adsorption (Ye et al. 2017). Chemical precipitation can usually reduce the concentration of P in a solution to a range of 0.5−1 mg L^{-1} (Mayer et al. 2013). It requires large quantities of metal ions, disposal of large quantities of sludge, and the recovery of metals is cumbersome, making this process suitable for treating effluents with higher P concentrations (Kumar et al. 2019). The EBPR process can theoretically reduce effluent P concentrations to 0.1−0.2 mg L^{-1} (Liu et al. 2019a, b). However, due to factors such as organic loading and reactor operating parameters, most EBPR

processes can only reduce P to 0.5−1 mg L^{-1} in actual projects (López-Vázquez et al. 2008). Microbial conversion is susceptible to environmental conditions, such as the organic carrier on which it is loaded, reaction vessel, and other factors (Wu et al. 2020). Adsorption is one of the most widely used P removal process, and it has a wide range of adsorbent materials, a fast P adsorption rate, high selectivity, a small amount of equipment input, and adsorbent regeneration (Desmidt et al. 2015).

Lanthanum (La) is a rare earth element (REE) having strong bonding ability with phosphate (Tang et al. 2019). Among the REEs, La is second only to cerium and neodymium in abundance in the earth's crust (Tyler 2004) and is widely used to adsorb P from water. However, because most P adsorption reactions involve monolayer adsorption (Wu et al. 2020), the aggregation of La can lead to a reduction in the adsorption capacity. Recently, researchers have chosen to load La onto inorganic carriers to avoid its leaching and aggregation, including activated carbon (Liu et al. 2022), carbon nanotubes (Zhang et al. 2022), and biochar (Chen et al. 2022; Liu et al. 2019a, b). Biochar is a carbon material produced by the thermal processing of biomass under limited oxygen conditions; when biochar is used as a soil amendment, it can serve to reduce soil density and enhance nutrient management. If the feedstock is biological waste with a disposal fee (Stávková and Maroušek 2021), the cost of recycling P does not increase, which in turn increases the economic attractiveness and competitiveness.

Shaddocks are a variety of pomelos that are widely grown in Southeast Asian countries. The mesocarp of shaddock refers to the part between the outer skin and the inner fruit, which is usually discarded as waste owing to the lack of food value. Therefore, it was selected as the raw material for biochar in this study. Given the strong binding ability of La to phosphate, it was hypothesized that the adsorption of P could be achieved by loading La on biochar. Therefore, one of the aims of this study was to verify the adsorption effect of P in an aqueous environment by the shaddock mesocarp biochar after loading of La and whether it could enhance the water quality of eutrophic water bodies. In addition, since biochar can be used as a soil amendment, another aim was to verify whether the adsorbent waste after P adsorption could be used as an effective slow-release P fertilizer to improve soil fertility and plant growth. In conclusion, the material prepared in this study may be a promising P sorbent for application, and it is also hoped that the research methods used in this paper can provide some ideas for scholars in related fields.

2 Material and methods

2.1 Reagents and formulae
The reagents used in this study are described in detail in the Additional file 1, and the relevant formulae used in this study are listed in Additional file 1: Table S1.

2.2 Adsorbent preparation
The method of preparing biochar with the mesocarp of shaddock (MSB) is described in the Additional file 1. MSB (3 g) was sonicated and dispersed in 500 mL of water to form a suspension, and 1 g of LaCl$_3$·7H$_2$O was dissolved in 100 mL of water and added to this suspension. The suspension was stirred at 1000 rpm for 10 h and ammonia was added dropwise until the pH of the mixture reached 11. After 12 h of stirring, the solid was collected by filtration, and the filter cake was washed with water to neutral pH and dried under vacuum at 80 °C for 6 h. The product was named MSBL1. Other conditions were kept constant, and only 1 g of LaCl$_3$·7H$_2$O was replaced with 2, 3, and 4 g to obtain MSBL2, MSBL3, and MSBL4, respectively. A schematic diagram of the preparation of the shaddock mesocarp for La-loaded species is shown in Fig. 1a. After going through the processes of peeling, freeze-drying, heat treatment, and La loading in turn, the P absorbing agent was successfully prepared.

2.3 Adsorbent characterization
The preparation of the adsorbents at different ratios and the mechanism of adsorption of P by MSBL3 were analyzed using Powder X-ray diffraction (PXRD), Brunauer–Emmett–Teller theory (BET), X-ray photoelectron spectroscopy (XPS), scanning electron microscopy (SEM), transmission electron microscopy (TEM), spherical aberration corrected transmission electron microscope (ACTEM), and other methods. The instrument models are described in the Additional file 1.

2.4 Batch adsorption experiments
P adsorption experiments were carried out in conical flasks, which were placed on a constant temperature water shaker at 150 rpm. Unless otherwise stated, the adsorbent dosage was 0.5 g L^{-1}, the reaction temperature was 25 ± 0.5 °C, initial P concentration was 50 mg L^{-1}, and initial pH of the solution was 7. A polytetrafluoroethylene rod of 0.5 cm diameter and 3 cm length was placed in a conical flask to ensure that the adsorbent did not collect at the bottom of the flask during centripetal oscillation. During the experiments, samples were collected at set time intervals and then filtered, after which the concentration of P in the water samples was determined using ammonium molybdate spectrophotometry and inductively coupled plasma-optical emission
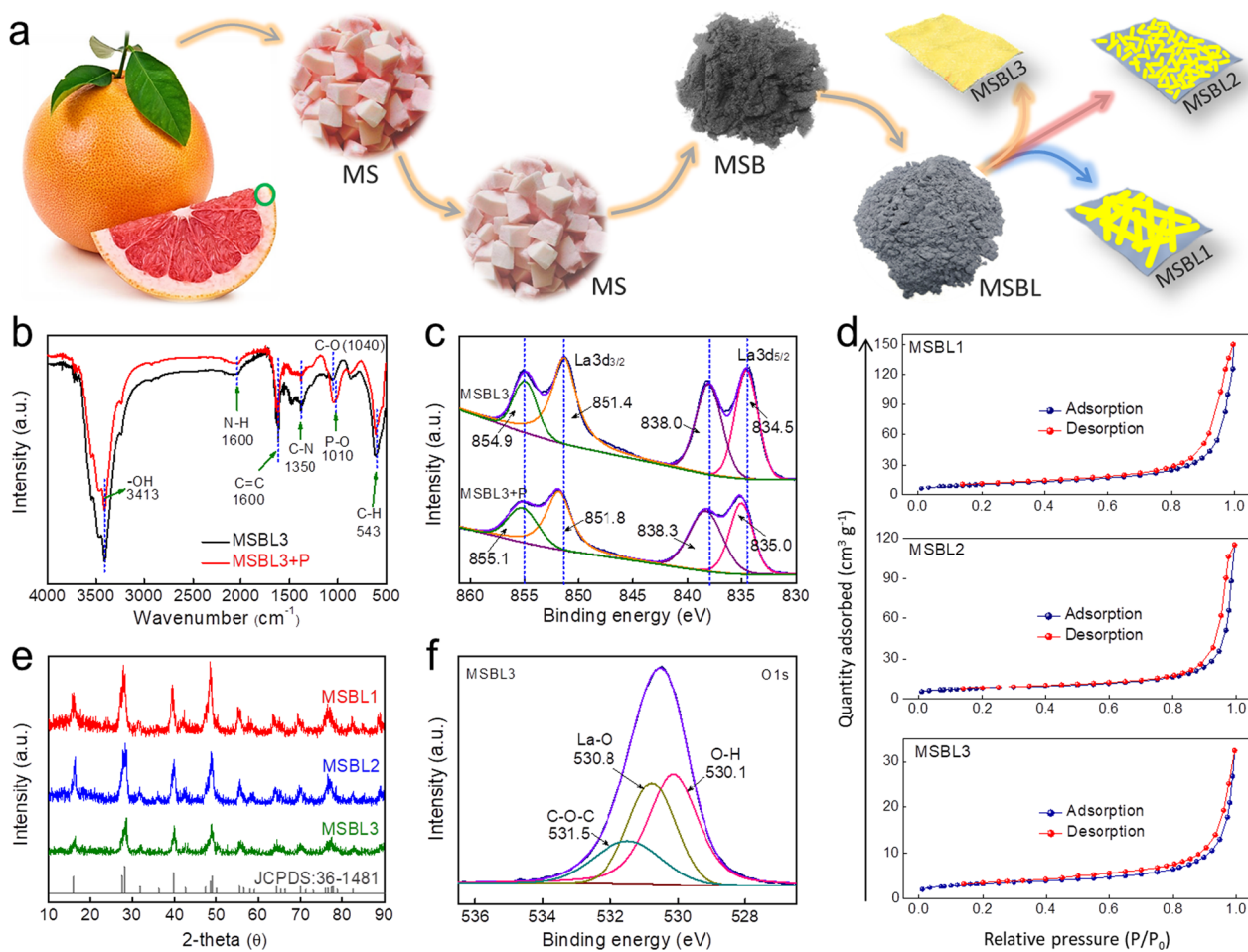
Fig. 1 **a** Preparation diagram of adsorbents; **b** FTIR spectra of MSBL3 and MSBL3 + P; **c** High-resolution XPS spectra of La 3d; **d** N$_2$ adsorption–desorption curve of adsorbents; **e** XRD pattern of adsorbents; **f** High-resolution XPS spectra of O1s

spectroscopy (ICP-OES), respectively. All experiments were performed in triplicate, and the results were reported as the mean with standard deviations.

When exploring the effect of co-existing ions, only the effect of ions with the same electrical properties as PO_4^{3-} was considered, where the cations were all K^+. The initial concentrations of CO_3^{2-}, NO_3^-, SO_4^{2-}, and Cl^- exhibited four different gradients (0 mg L^{-1}, 20 mg L^{-1}, 100 mg L^{-1}, and 200 mg L^{-1}), respectively. For the cyclic experiments, after each adsorption, the collected adsorbent was stirred in a NaOH solution (1 M) at 150 rpm for 10 h, washed to neutral pH, and dried. This procedure was repeated five times.

To assess the P sorption performance of the adsorbent in a natural water environment, water from different scenarios was used as a solvent for P, including ultrapure, municipal, lake, and river waters. Municipal water was collected from the municipal water supply network, lake water from *Dianchi* Lake, and river water from *Laoyu*

River, all located in Kunming, China. The insoluble material was filtered before preparing the P solution, and the P concentration in natural water was determined. On the other hand, the P concentration was set at three different gradients (5 mg L^{-1}, 10 mg L^{-1}, and 20 mg L^{-1}) using each of the four waters as solvent and the adsorbent performance in removing P was evaluated at neutral pH.

Continuous fixed-bed experiments were performed in an inorganic glass column with a length of 200 mm and outer diameter of 15 mm. Natural lake water samples were prepared as feed solutions with a P content of 2 mg P L^{-1}, and the flow rate was controlled using a peristaltic pump at 20 bed volume (BV) h^{-1}. The effluent solution was sampled at 0.5 h intervals. MSBL3 was desorbed in situ using a NaOH solution (1 M) as a resolving agent, and the adsorption–desorption process was repeated three times.

The eutrophication inhibition experiment using MSBL3 was set up with P-free, P-containing, and

P + MSBL3 groups, in which three different concentrations of P (20 mg P L^{-1}, 50 mg P L^{-1}, and 100 mg P L^{-1}) were set in the P + MSBL3 group. The effectiveness of MSBL3 on P adsorption and inhibition of eutrophication in water bodies was verified by comparing the growth status of water hyacinth.

The inhibitory properties of different MSBL3 concentrations against *E. coli* and *S. aureus* were also investigated. The antibacterial properties of MSBL3 were tested using the flat-plate coating method (Han et al. 2021; Yu et al. 2019a, b). First, MSBL3 was fully ground, and then the ground samples were wrapped in tin foil and dried for 20 min (120 °C, dry heat sterilization of materials). *E. coli* and *S. aureus* were placed in shake flasks filled with Luria–Bertani (LB) agar medium for 18 h (180 rpm, 35 °C). To prepare the inoculum, the cultured *E. coli* and *S. aureus* solutions were diluted to 10^{-7} and 10^{-8}, respectively. 8 mg of sterilized MSBL3 was added to 10 mL of LB liquid culture medium to obtain a concentration of 0.0001 M MSBL3. Similarly, the concentrations of MSBL3 with 0.001 M, 0.01 M and 0.1 M were obtained with corresponding sterilized MSBL3.

Maize was chosen as the target plant for the resource-planning experiment after sorbent fatigue. According to the Chinese soil classification standard (GB/T 17296-2009), the type of soil in this study was *Lateritic red soil*, which is widely distributed in the southern half of China and is a clayey soil with poor fertility. The physicochemical characteristics of the soils are list in Table 1. Maize seed is the *national trial high-yielding zhengdan 958*, which is characterized by its salinity and drought tolerance. The seeds were soaked in warm water at approximately 55 °C for 8–12 h before planting. The seeds were kept at a cultivation temperature of 23 ± 3 °C, soil humidity of 40–60%, air humidity of 40–50%, and light at 10 ± 2 h per day. The growth conditions were kept consistent and the growth of maize in soil samples doped and un-doped with MSBL3 was compared to verify whether MSBL3 could be recycled directly back into the soil as an effective slow release P fertilizer after the adsorption of P reached the fatigued state.

Additional experimental procedures, statistical analyses, and results are described in the Additional file 1.

3 Results and discussion

3.1 Idea of material selection

There was a thick fluffy mesocarp between the shaddock peel and pulp, which was considered useless and discarded together with the shaddock peel. In terms of environmental management, it is expected that cheap and readily available biomass can be locally sourced for conversion to useful biochar. Considering that the mesocarp in the shaddock peel and pulp sandwich exhibits a fluffy and porous state from a macro perspective, we used it as a biochar carrier for La species that can effectively remove P.

3.2 Physicochemical state and morphology of adsorbents

The FTIR spectrum (Fig. 1b) shows that the MSBL contains a rich variety of functional groups, such as –OH, –N–H, C–N, and C–O (Wang et al. 2020). These species are present in most biochar materials and can significantly influence the physicochemical properties of biochar, for example, by anchoring metallic species (metals or their compounds), changing the electrical properties of the biochar surface, or acting as hydrogen bond acceptors (or donors). In the powder X-ray diffraction (PXRD) spectrum (Fig. 1e), MSBL1, MSBL2, and MSBL3 exhibited signal peaks that were consistent with the crystalline phase of La(OH)$_3$ with a crystal group of P63/m (JCPDS:36-1481). Thus, a gradual increase in ammonia input allows for an increase in the pH of the solution, with La^{3+} forming La(OH)$_3$ insoluble matter in a stronger alkaline environment and loading onto the MSB biochar. In addition, the PXRD peak weakened with increasing amounts of LaCl$_3$. This phenomenon may be related to the size of the La(OH)$_3$ crystals formed; the higher the LaCl$_3$ concentration, the smaller the La(OH)$_3$ particles obtained in the presence of ammonia. The XPS spectra were compared to the PXRD spectra. The chemical valence of La in MSBL (in the case of MSBL3) was + 3. The signals at 834.5 eV and 838.0 eV were attributed to La3d$_{5/2}$, and the signals at 851.4 eV and 854.9 eV were attributed to La3d$_{3/2}$ (Fig. 1c). The satellite peaks of La3d$_{5/2}$ and La3d$_{3/2}$ of MSBL3 were at high binding energies and had strong signals, which may be related to the shake-up process resulting from the charge transfer between O2p-La4f. In the O binding energy region, the

Table 1 The soil physicochemical characteristics

	Colour	Structure	pH	Organic carbon (g kg^{-1})	Total P (g kg^{-1})	Available P (mg kg^{-1})
Blank control soil	Brick red	Granular	5.95	2.951	0.674	6.000
Soil + MSBL3	Greyish red	Granular	5.89	30.057	7.221	83.250

XPS-acquired signal peaks can be obtained by coupling three fitted peaks at 530.1 eV, 530.8 eV, and 531.5 eV, which correspond to the signals of the O–H, La–O, and C–O–C bonds (Yang et al. 2019), respectively (Fig. 1f). In addition, the effect of different $LaCl_3$ dosages on the specific surface area of the biochar was derived from the nitrogen adsorption and desorption curves of MSBL1, MSBL2, and MSBL3.

The specific surface areas (based on BET analysis) of MSB, MSBL1, MSBL2, and MSBL3 were obtained from the nitrogen adsorption and desorption curves as 59.5, 39.5, 27.8, and 11.8, respectively. Clearly, the BET surface area of MSB decreased when loaded with $La(OH)_3$, and this decreasing trend became more pronounced as the amount of $LaCl_3$ input increased. This may be due to the introduction of $La(OH)_3$, resulting in the filling and covering of the original pore and base surfaces of the MSB, leading to a continuous decrease in the BET values (Fig. 1d). It is worth noting that the introduction of $La(OH)_3$ fills the pore channels of the MSB to some extent and therefore the average pore sizes reported in MSBL1, MSBL2, and MSBL3 should be derived from the statistical results of the interstitial spaces between the $La(OH)_3$ species. In the above discussion, the PXRD signal indicates that the larger the $LaCl_3$ input, the smaller the $La(OH)_3$ particles that are likely to be formed and, therefore, more uniformly distributed. In this case, the gaps between the smaller particles
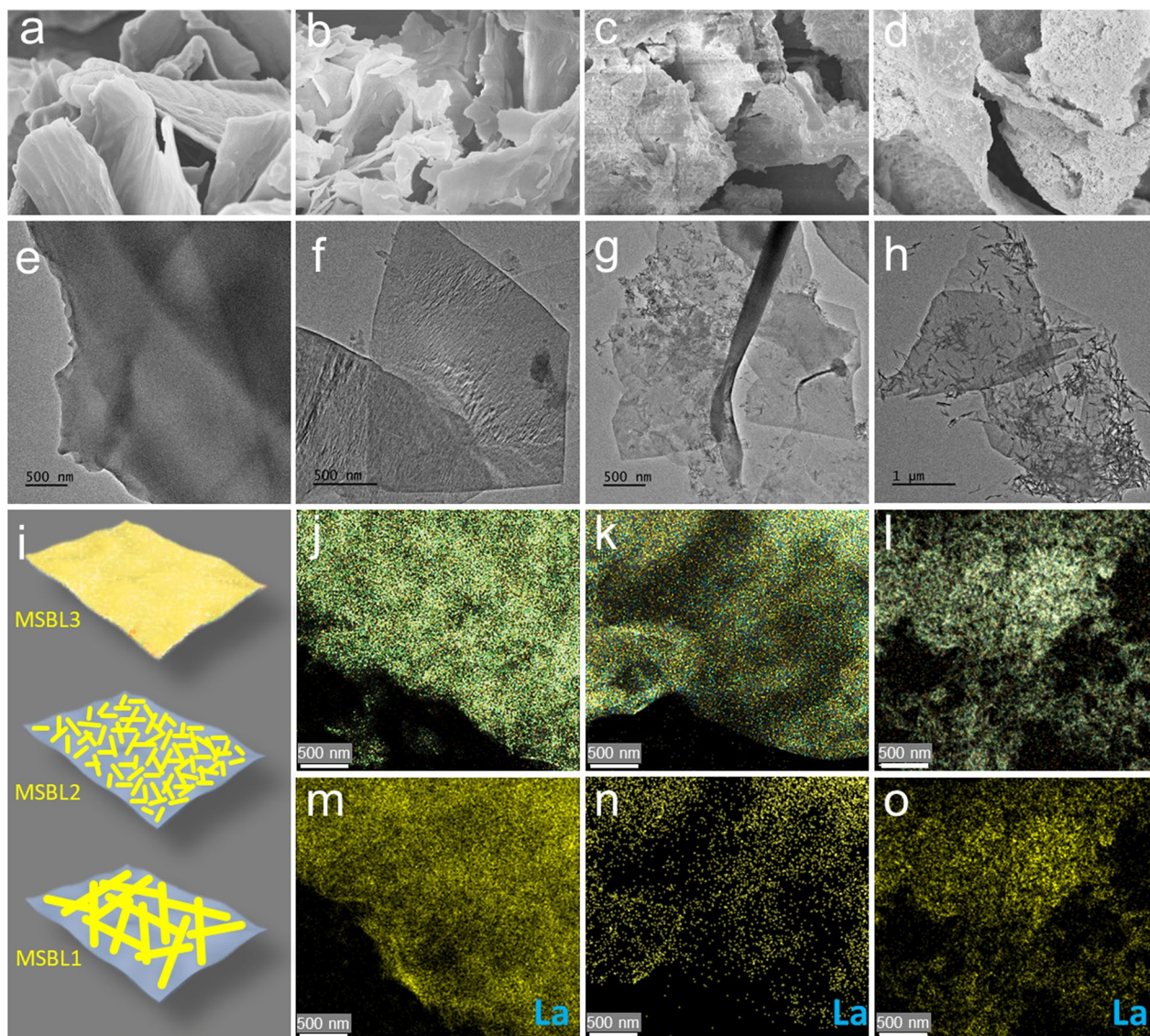

Fig. 2 SEM images of MSB (**a**), MSBL3 (**b**), MSBL2 (**c**), and MSBL1 (**d**); TEM images of MSB (**e**), MSBL3 (**f**), MSBL2 (**g**), and MSBL1 (**h**); (**i**) Schematic diagram of adsorbents morphology; EDS element mapping of MSBL3 (**j**, **m**), MSBL2 (**k**, **n**), and MSBL1 (**l**, **o**)

of La(OH)$_3$ were tighter; therefore, the pore size was smaller.

Electron microscopy imaging directly presents the microscopic morphological features of the MSBL. Figure 2a, e shows the SEM and TEM images of the MSB, respectively. MSB had a slightly distorted two-dimensional lamellar structure with a smooth and delicate base. When loaded with La(OH)$_3$, the SEM and TEM images of MSBL3 (Fig. 2b, f) were similar to those of MSB, and it was difficult to distinguish the formation of new material on the base surface of the biochar with the naked eye. The difference is that, although the morphologies of both MSBL2 (Fig. 2c, g) and MSBL1 (Fig. 2d, h) were two-dimensional lamellar structures, the lamellar base surface became rough, and the roughness of MSBL1 was more pronounced than that of MSBL2. In the TEM images, a large number of nanorods were attached to the MSB surface in MSBL2 and MSBL1, the length of the nanorods in MSBL2 was approximately 100 nm and that in MSBL1 was approximately 400 nm. Because the MSB surface was smooth and without any rods, the nanorods on the MSB substrate in MSBL2 and MSBL1 were La(OH)$_3$ species.

Elementals C, N, O, and La were all distributed in MSBL3 (Fig. 2j, m), MSBL2 (Fig. 2k, n), and MSBL1 (Fig. 2l, o) based on elemental mapping imaging. The La signal was more uniformly distributed on MSBL3, whereas it was the least distributed on MSBL1. However, it was difficult to observe any new species in the TEM images of MSBL3, where the morphology could be resolved. It was observed that the particle size of the La species (characterized as La(OH)$_3$ by PXRD) gradually decreased as the amount of LaCl$_3$ input increased. Thus, the nanorods in MSBL1 had a larger particle size than those in MSBL2, whereas the La(OH)$_3$ particles in MSBL3 may be uniformly distributed to form a homogeneous film on the MSB surface (Fig. 2i). To test this hypothesis, we used a more accurate ACTEM to observe the microscopic morphology of the MSBL3.

When the scale bar reached 200 nm and 20 nm, the surface of the flake carrier of MSBL3 remained smooth (Fig. 3a, b). However, when the field of view was enlarged to a scale bar of 10 nm, various new species with good crystallinity in the size (planar size) range of 2−10 nm were seen distributed on the MSB surface, which were
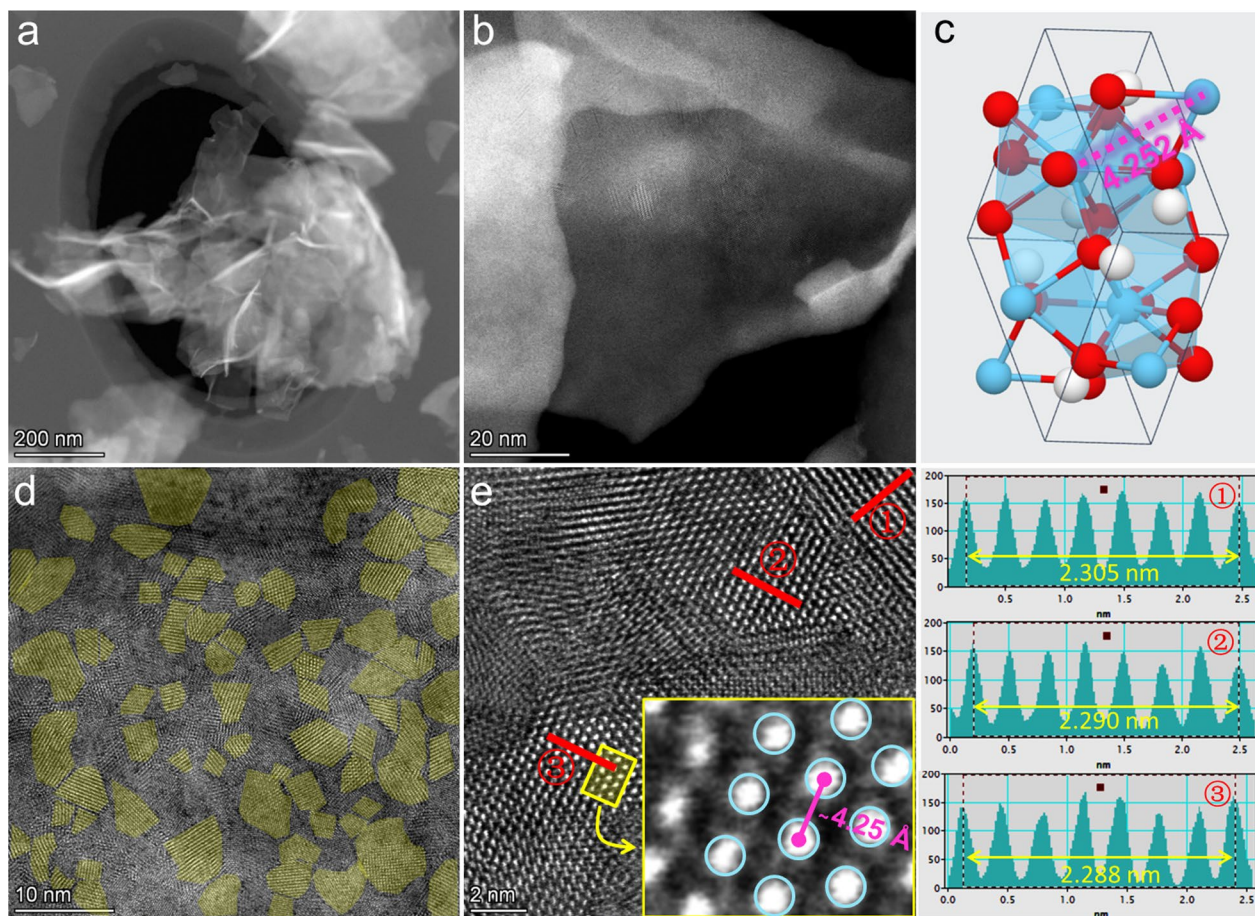

Fig. 3 AC-HRTEM with HAADF mode (**a**, **b**, **d**, **e**) of MSBL3; (**c**) crystal lattice model and lattice spacing of La(OH)$_3$ on MSBL3

closely connected to each other with almost no obvious fault lines (Fig. 3d). The lattice spacing of these new species was close to 0.326 nm, which is consistent with the lattice spacing of the 110 crystal face of La(OH)$_3$. Therefore, the new species evenly distributed on the MSB was La(OH)$_3$. Using the high-angle annular dark field (HAADF) image mode, it can be inferred that the bright spots of atomic size in the lattice stripe in Fig. 3e are La atoms because of the stronger scattering of electrons by metal atoms with larger atomic numbers. It can be found that the distance between adjacent bright spots on the lattice line is about 4.25 Å, which is consistent with the La-La distance in the La(OH)$_3$ crystal cell (Fig. 3c). This evidence effectively verifies the above reasonable hypothesis that the particle size of La(OH)$_3$ on MSB is small in the order of MSBL1, MSBL2, and MSBL3, and that its distribution on MSBL3 exhibits a high dispersion of small particle sizes.

3.3 Performance study of P removal

In detail, the ability of La(OH)$_3$ loaded onto MSBs to adsorb P species from water was evaluated. The pH of natural water is close to neutral; therefore, the ability of MSBL1, MSBL2, MSBL3, and MSBL4 to adsorb P in P solutions at pH7 (P concentration of 50 mg L^{-1}) was first evaluated. When the adsorption reached equilibrium, the P adsorption capacities of MSBL1, MSBL2, MSBL3, and MSBL4 were 27.4 mg P g^{-1}, 41.8 mg P g^{-1}, 60.5 mg P g^{-1}, and 62.1 mg P g^{-1}, respectively (Fig. 4a).

In general, La(OH)$_3$ exhibits good adsorption of P species (e.g. phosphate) in water. The loading of La(OH)$_3$ in MSBL1, MSBL2, and MSBL3 gradually increased, so that their P adsorption capacity gradually increased, in line with theoretical predictions. However, compared to MSBL3, MSBL4 did not significantly increase the adsorption capacity of P. Therefore, considering the effect of P adsorption and economic benefits, MSBL3 was the only experimental group used for subsequent batch experiments. In view of the complexity of the water column, the effect of pH on P adsorption by MSBL3 was investigated, and the adsorption capacity of P varied with the pH of the solution (Fig. 4b). The maximum P adsorption capacity of MSBL3 was 78.5 mg g^{-1} when the pH was approximately 3. When the pH was below 3, the P adsorption capacity of MSBL3 decreased sharply, which may be related to the dissociation of La(OH)$_3$ in a strongly acidic environment. When the pH was higher than 3, the adsorption capacity of MSBL3 for P slowly decreased, and this trend became more pronounced when the pH was higher than 7 (Yin et al. 2022). The zeta potential distribution (Fig. 4e) of MSBL3 shows that its surface electrostatic potential was positive when the pH was below 10. When the pH increased from 10 to 11, the MSBL3 surface electrostatic potential reversed from positive to negative (Jia et al. 2022). It can be assumed that a positive electrostatic potential indicates more H$^+$ enrichment or the presence of more protonated groups (e.g. NH$_4^+$) on the material surface, whereas a negative electrostatic
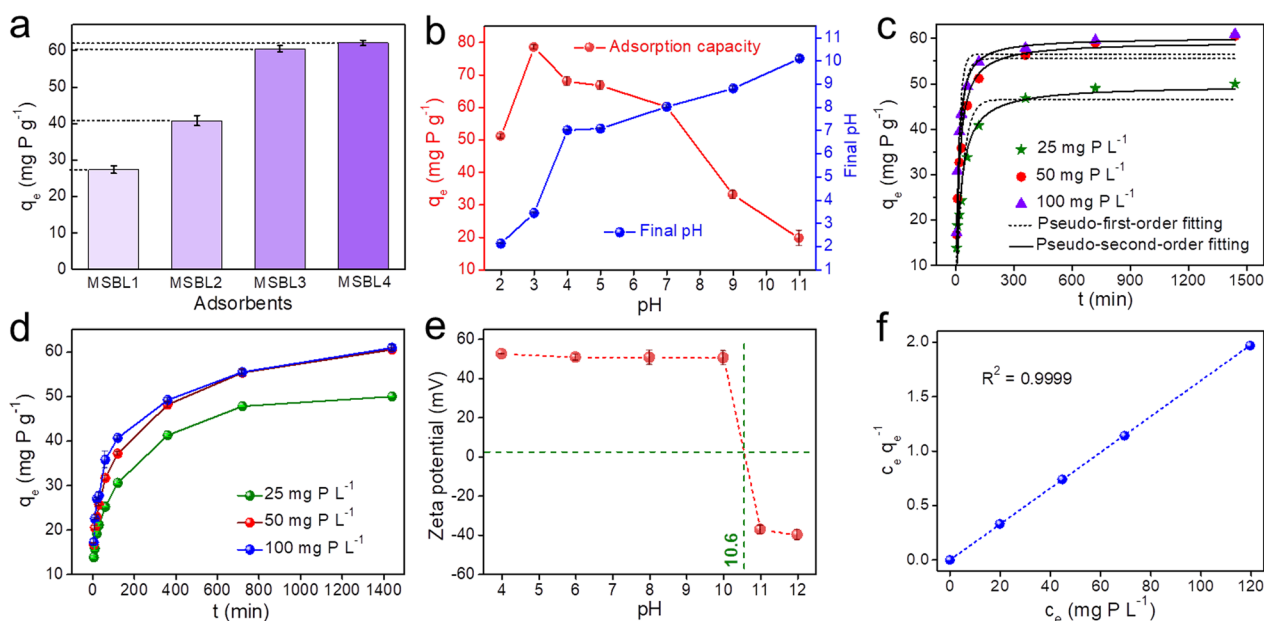

Fig. 4 **a** Comparison of q$_e$; **b** Effect of initial solution pH on P removal of MSBL3; **c** Sorption kinetic models; **d** Effect of different P concentrations on q$_e$; **e** Zeta potential of MSBL3; **f** Langmuir model. (dosage of adsorbent: 0.5 g L^{-1}; T: 298 K)

potential indicates more OH$^-$ enrichment on the material surface (Wang et al. 2021a, b). As the pH gradually increased from 3, the OH$^-$ content of the solution gradually increased, which weakened the H$^+$ or protonated groups on the material surface. This weakened the Coulombic interaction of the negatively charged PO$_4^{3-}$ (or HPO$_4^{2-}$ and H$_2$PO$_4^-$) with the material surface, thus reducing the adsorption capacity of MSBL3 for P (Wang et al. 2021a, b).

Based on the adsorption capacity–time curve (Fig. 4d), the adsorption behavior of P on MSBL3 can be explained using pseudo-first-order and pseudo-second-order kinetic models (Fig. 4c), that is, physical adsorption and chemical adsorption, respectively. The regression coefficients (R^2) fitted by the pseudo-first-order model were lower than those of the pseudo-second-order model (Additional file 1: Table S2). Therefore, the adsorption of P on MSBL3 was more consistent with the pseudo-second-order kinetic model, and was mainly chemisorption. In addition, the attachment state of P to MSBL3 was investigated using Langmuir and Freundlich models. When the Freundlich model was fitted linearly to the isothermal adsorption data, the value of R^2 was only 0.801 (Additional file 1: Fig. S1b), whereas the value of R^2 obtained when the Langmuir model was used to fit the isothermal adsorption data was 0.999 (Fig. 4f). Thus, the Langmuir model is more consistent with the P attachment behavior of MSBL3 as a single molecular layer.

3.4 Universality of practical application of adsorbent
3.4.1 Practicality verification of MSBL3
Before the practical application of the adsorbent, it is necessary to consider its effects, such as the type of actual water and co-existing ions. Water samples were collected from nearby waters and tested for P concentrations, with P concentrations of 3.0 μg L^{-1} and 24.0 μg L^{-1} in samples collected from *Dianchi* Lake and *Laoyu* River, respectively (Fig. 5a). After adsorption by MSBL3, P was not detected in either water sample; therefore, the removal efficiency was 100%. Ultra-pure water, municipal water, *Dianchi Lake* water, and *Laoyu River* water samples were used as solvents to prepare solutions with concentrations of 5 mg P L^{-1}, 10 mg P L^{-1}, and 20 mg P L^{-1}, respectively. At a concentration of 20 mg P L^{-1}, the removal efficiency of P by MSBL3 reached more than 99.9% for the first two water samples, whereas for *Dianchi* and *Luoyu River* water samples, it was 94.5% and 94.1%, respectively, which might be due to the presence of other competing ions in the lake water samples that would inhibit P removal to some extent (Fig. 5b).

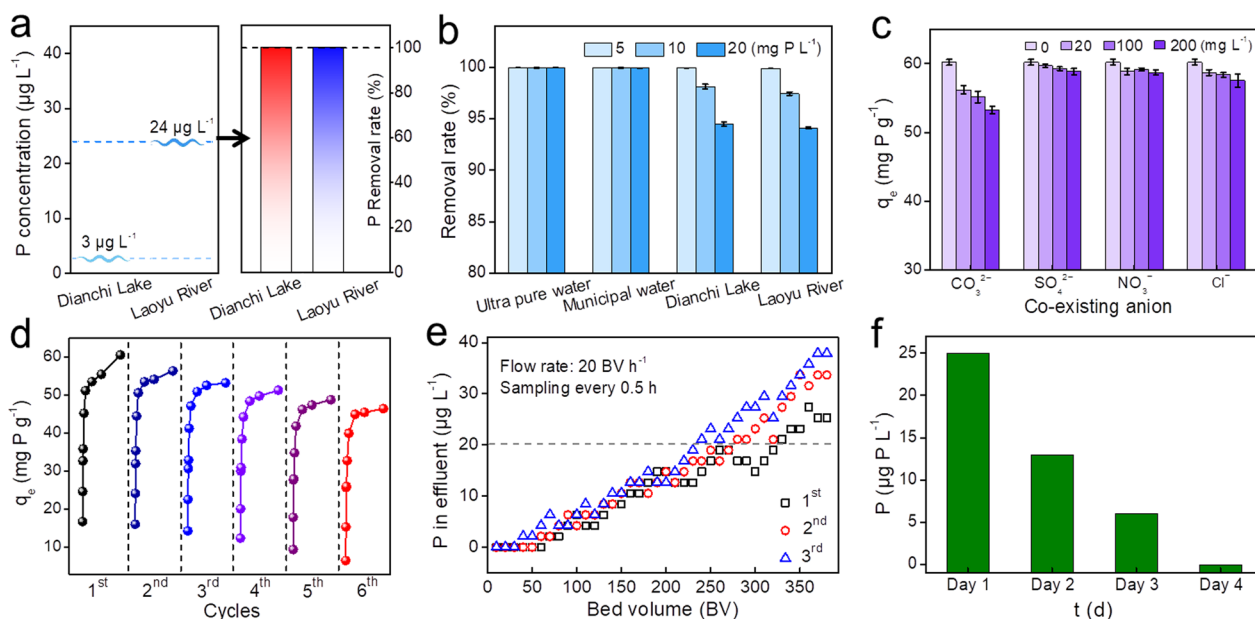The presence of co-existing anions such as CO$_3^{2-}$, SO$_4^{2-}$, NO$_3^-$, and Cl$^-$ in the P solution did not

Fig. 5 **a** Adsorption of P by MSBL3 in natural water; **b** Adsorption of P in four water bodies by MSBL3 (Solutions of 5, 10, and 20 mg P L^{-1} were prepared using the four water samples as diluents); **c** Effect of coexisting anions on q$_e$; **d** Adsorption–desorption cycles. (dosage of adsorbent: 0.5 g L^{-1}; T: 298 K); **e** P concentration in the effluent at different cycles. (C$_0$: 2 mg P L^{-1}; dosage of MSBL3: 0.25 g; T: 298 K); **f** Adsorption effect of magnification experiment (Volume of P solution: 25 L; dosage of MSBL3: 2.5 g; C$_0$: 25 μg L^{-1}; T: 298 K; The Y-axis represents the concentration of P in the solution)

significantly affect the performance of MSBL3 for P adsorption (Fig. 5c). The high selectivity of MSBL3 for PO_4^{3-} (or HPO_4^{2-} and $H_2PO_4^-$) can be explained by the fact that the products $LaCl_3$, $La(NO)_3$ and $La_2(SO_4)_3$ formed by La^{3+} with Cl^-, NO_3^-, and SO_4^{2-} are all water-soluble compounds and, therefore, have a small tendency to react with MSBL3. When the co-existing ion was CO_3^{2-}, the adsorption of P by MSBL3 slightly decreased because La^{3+} easily combined with CO_3^{2-} to form a $La_2(CO_3)_3$ solid, but the pKsp of $La_2(CO_3)_3$ was smaller than that of $La(OH)_3$, making it difficult for CO_3^{2-} to capture most of the La^{3+} sites (Yu et al. 2019a, b).

Reproducibility of the adsorbent is particularly important for practical applications. Considering the complete conversion of $LaCl_3$ to $La(OH)_3$ on MSB, NaOH can be used to provide a significant amount of OH^- to reconstitute the $La(OH)_3$ species after P adsorption by MSBL3. After six repeated uses, MSBL3 was able to retain 76.7% of its initial performance in terms of P adsorption capacity (Fig. 5d), which is better than that of most reported P adsorbents, making MSBL3 economically relevant in practical applications.

3.4.2 Continuous fixed-bed column experiment
A fixed-bed adsorption experiment was designed to investigate the potential of the PL adsorbent for application in flowing lake water. Both ends of the tower were equipped with layers of quartz sand plates to prevent PL loss (Additional file 1: Fig. S4). The water sample collected from the *Laoyu* River was used as the feed solution. To visually verify the adsorption effect of PL in natural water, the initial P concentration in the water sample was adjusted to 2 mg P L^{-1}.

The breakthrough point for P was set at 20 μg L^{-1} because exceeding this value could result in lake eutrophication (Yao et al. 2013). As shown in Fig. 5e, the first adsorption experiment reached a breakthrough point at a water volume of 330 BV, and q_e was 29.3 mg P g^{-1}. Subsequently, a 1 M NaOH solution was used to desorb PL in a cyclic manner until the P concentration in the desorbed solution became constant, which took approximately 5.5 h. After desorption, MSBL3 was rinsed with deionized water until the effluent was neutral, after which the next cycle was initiated. The breakthrough point reached 280 BV and 240 BV for the second and third times, respectively, with q_e of MSBL3 for P being 24.8 mg P g^{-1} and 21.3 mg P g^{-1}, respectively. The third time, q_e was 72.6% of the initial value. In addition, the leakage of La in the first effluent was 207.7 μg L^{-1} and 89.5 μg L^{-1} after the third cycle. Although there is no standard limit for La in the Chinese surface water environmental quality standard, it is unclear whether La leaching will have a negative impact on the ecological environment. Therefore, it is necessary to focus on reducing La leakage from the adsorbent in subsequent studies. For example, improving the preparation method to firmly fix La in the adsorbent or reducing the loading of La while ensuring the removal efficiency of P.

3.4.3 Magnification experiment
In practical applications, the separation cost after the reaction is considerably higher if the powdered adsorbent is sprayed directly in water. Additionally, incomplete separation produces a large amount of sludge. Therefore, we conducted a scale-up experiment to reduce the separation cost of the adsorbent and meet the practical application requirements. As shown in Additional file 1: Fig. S5, filter packages containing MSBL3 were dosed into the P-containing water. Owing to the low mobility of the lake water, the water box was shaken slightly at fixed times to simulate water flow. Samples were taken at fixed times each day and the P content of the solution was measured. As shown in Fig. 5f, after three days, P was not detected in the solution. It can be seen that loading the adsorbent in the filter pack will prolong the time required for the reaction due to uneven dispersion, but will still achieve the effect of adsorbing P. A filter package containing MSBL3 can be easily removed after the adsorption is complete, which is more practical and allows for a wide range of applications.

In terms of economic cost analysis, biomass is abundant in nature and is environmentally and economically sustainable (Maroušek and Maroušková 2021). In this study, biochar was doped with La, which, although classified as a rare earth element, is abundant in the earth's crust, second only to cerium and neodymium. Because of the high requirements for elemental purity in the preliminary tests, analytically pure $LaCl_3·7H_2O$ was chosen, which is slightly more expensive at 132.6 RMB 500 g^{-1}. The preparation of 1 g of MSBL3 requires 0.7 g of $LaCl_3·7H_2O$, 0.7 g of mesocarp of shaddock, and 25 mL of $NH_3·H_2O$. The cost of the above reagents, in addition to the water and electricity used throughout the process, is approximately 1 RMB, and it can reduce the P concentration in 2.6 ton of *Laoyu River* water to below the eutrophication threshold. Although this cost is not very high, it is necessary to continue to reduce the cost if large-scale practical applications are to be achieved (Durana et al. 2021; Maroušek and Trakal 2022). Market research shows that commercially available $LaCl_3$ sells for only 17 RMB kg^{-1}, a difference of approximately 15 times the price of the analytically pure grade, hence this is commercially promising.

3.4.4 Inhibition of eutrophication in water bodies by MSBL3

In eutrophic water bodies, algae and water hyacinth grow in large numbers, aggravating the deterioration of the water body. If P in a water body can be reduced below the eutrophication threshold, the occurrence or deterioration of eutrophication in the water body can be effectively avoided. Therefore, we investigated the inhibitory effect of placing MSBL3 in P-containing water on the growth of water hyacinth. As shown in Fig. 6, during 25 d of incubation, all water hyacinths in the group containing P grew well, with a significant increase in the number of leaves; and most leaves were bright green. Higher the P content, greater the number of new leaves; however, when the P concentration was increased to 100 mg L^{-1}, there was no significant increase in the number of leaves, along with the presence of slightly more old leaves. This suggests that too high a P concentration would have an inhibitory effect on growth. The growth trends of water hyacinth in the MSBL3 and P-free groups were similar, and by day 25, the leaves had died in large numbers and new leaf growth was insignificant. This verifies the effectiveness of MSBL3 for P adsorption and shows that MSBL3 has an inhibitory effect on the growth of water hyacinth. It can be effectively used to prevent eutrophication in water bodies and can also be applied to eutrophic water to inhibit the excessive growth of water hyacinth or algae, alleviate the level of eutrophication, and maintain the ecological balance of water.
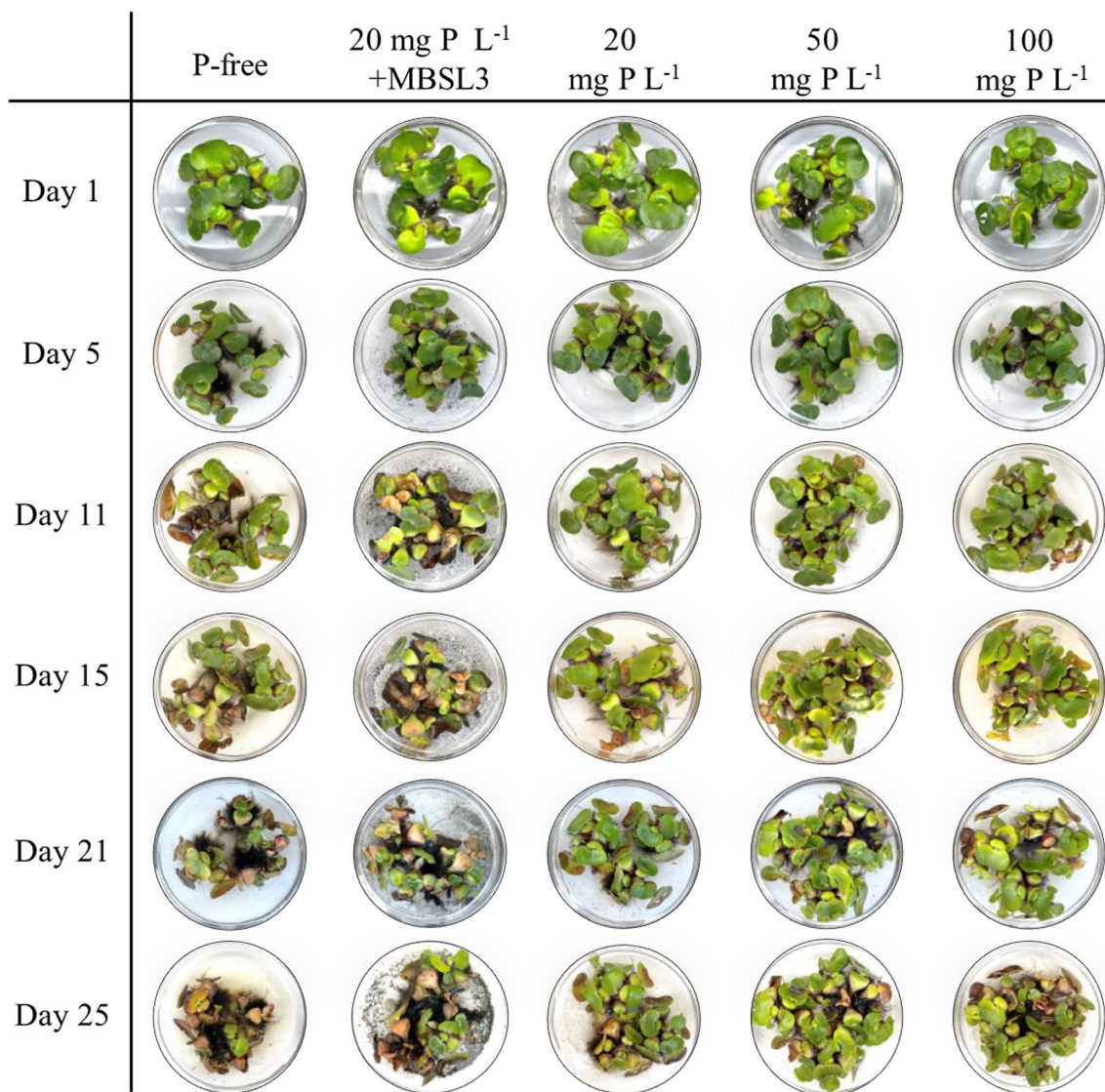

Fig. 6 The growth trend of water hyacinth at different P levels

3.4.5 Antibacterial test

A number of P-containing water bodies, such as livestock wastewater (Wang et al. 2021a, b), urban sewage plant wastewater (Bonetta et al. 2016), and even water networks (Holinger et al. 2014), contain large amounts of bacteria; therefore, if the adsorbent can act as a bacterial inhibitor in the process of P removal, then this material can achieve both P recovery and improved water quality. Therefore, *E. coli* and *S. aureus*, which are commonly found in water bodies, were chosen as the target species to assess the bacterial inhibition performance of MSBL3. As shown in Fig. 7b, c, the growth of *E. coli* and *S. aureus*, was barely inhibited when MSBL3 was excluded. Compared to the blank group, when the concentration of MSBL3 was 0.0001 M, the inhibition against *E. coli* and *S. aureus* was 87.3% and 75.0%, respectively. When the concentration of MSBL3 reached 0.1 M, inhibition against both bacteria reached 98.7% and 85.0%, respectively. This may be because MSBL3 is rich in functional groups,

such as positively charged NH_4^+, and the cell membrane surface of bacteria is negatively charged; therefore, it can attract more bacteria through electrostatic gravity, causing a large loss of cytoplasmic components and disrupting their normal physiological function, leading to bacterial death (Wei et al. 1994). The above results show that MSBL3 can inhibit the growth of *E. coli* and *S. aureus* in the water column; therefore, the application of MSBL3 to recover P from the water column can simultaneously improve water quality at the same time.

The inhibitory effects of MSBL3 on *E. coli* and *S. aureus* involve two main mechanisms. The first is direct inhibition. Studies have shown that La ions have an inhibitory effect on microbial growth. When the concentration of La ions was 1000 $\mu g\ L^{-1}$ and 100 $\mu g\ L^{-1}$, respectively, it was able to kill 83% and 39% of *E. coli* in just 1 min (He et al. 2015). In this study, the leaching amount of La in MSBL3 was approximately 200 $\mu g\ L^{-1}$, which would
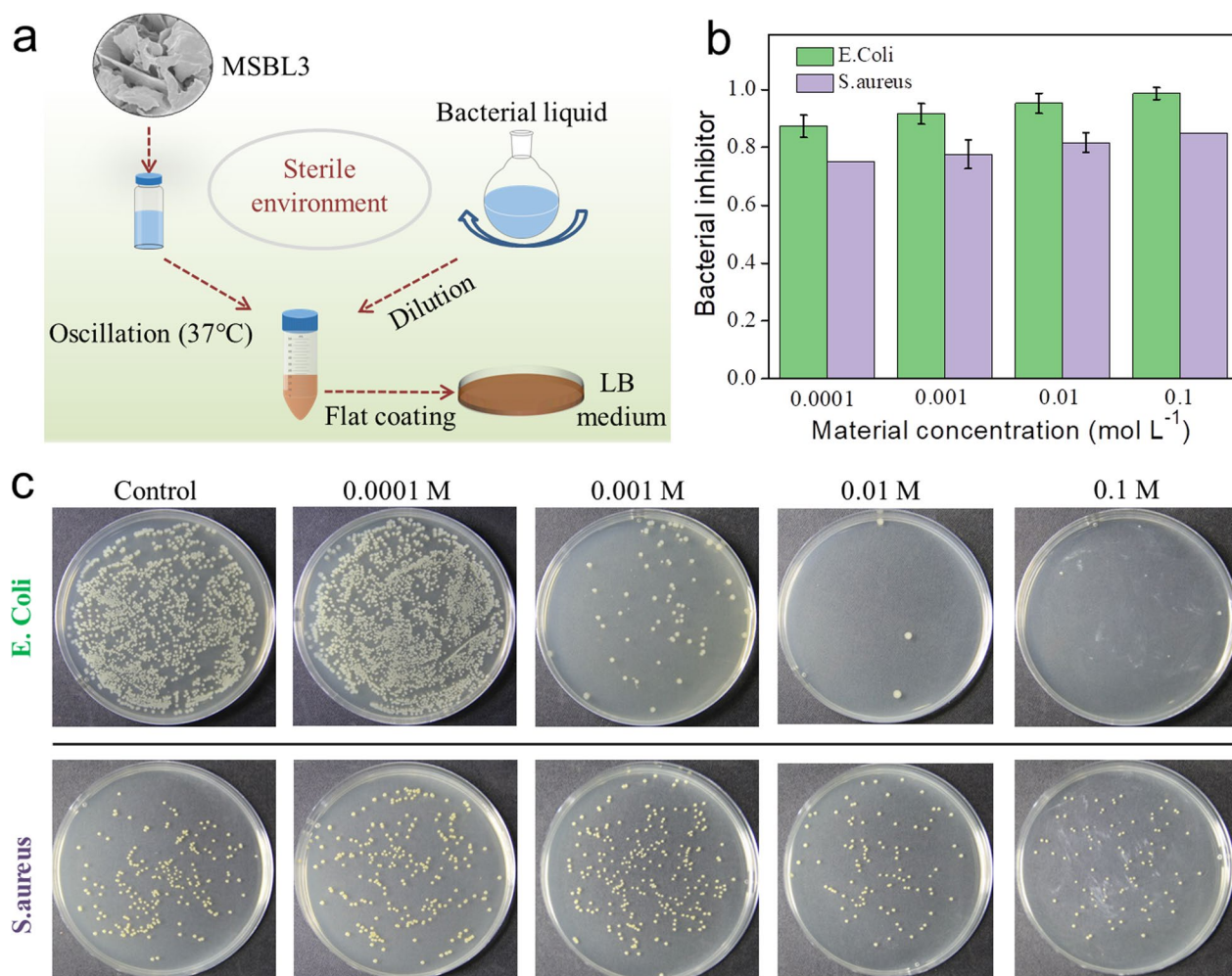

Fig. 7 **a** Flow chart of the antibacterial test; **b**, **c** Inhibition of E. coli and S. aureus at different concentrations of MSBL3

directly inhibit bacterial growth to some extent. The second is indirect inhibition: in the growth of bacteria, phosphorus and organic carbon sources serve as nutrients for their growth and reproduction, and if the P source is controlled, the growth of bacteria is inhibited (Zhang et al. 2016). In this study, the significant adsorption of P by MSBL3 resulted in "P deficiency" and some microorganisms were unable to perform normal metabolism in this P-deficient environment, which led to their death.

3.5 Resource planning after adsorbent fatigue

Adsorption is a simple and effective strategy for pollutant treatment, but it often faces problems such as difficulties with post-treatment of the adsorbent sludge. However, when the adsorbent is used several times, its ability to adsorb pollutants decreases. When it reaches its maximum service life, adsorbent sludge causes secondary pollution to the environment and its disposal is costly (Sornhiran et al. 2022). In this study, MSBL3 was the biomass material, and when it was enriched with P in solution, it formed a complex with compositional properties similar to those of grass ash, which has a fertilizing effect. Therefore, when MSBL3 reaches its final fatigue state, it can be placed directly on nutrient-poor agricultural land, instead of separating MSBL3 from P. This will

reduce the cost of treating pollutants by adsorption and has the potential to add value to the waste resources of adsorbent sludge. Therefore, we investigated the viability of MSBL3 as a fertilizer for agricultural fields, following the adsorption of P species in water. Considering the high dependence of maize on P during growth, the growth of maize seeds in soil samples, with and without MSBL3, was studied. The other growth conditions were kept consistent and maize growth was recorded at the same time each day. As shown in Fig. 8, maize seeds started to sprout on the eighth day, and the growth rate of maize in the soil samples without MSBL3 was considerably slower than that in the soil samples with MSBL3. After a few days, the maize seedlings in the MSBL3-doped group were tall and thick, whereas those in the non-MSBL3-doped group were short and thin. Therefore, it can be tentatively determined from the growth status of corn seedlings that MSBL3 can be used as an effective slow-release P fertilizer.

However, it has been demonstrated that moderate amounts of La can also have beneficial effects on plant growth, such as promoting photosynthesis and accelerating growth (Agathokleous et al. 2018). Therefore, the availability of P for plant nutrition in this study needs to be investigated further. The availability of P and La for
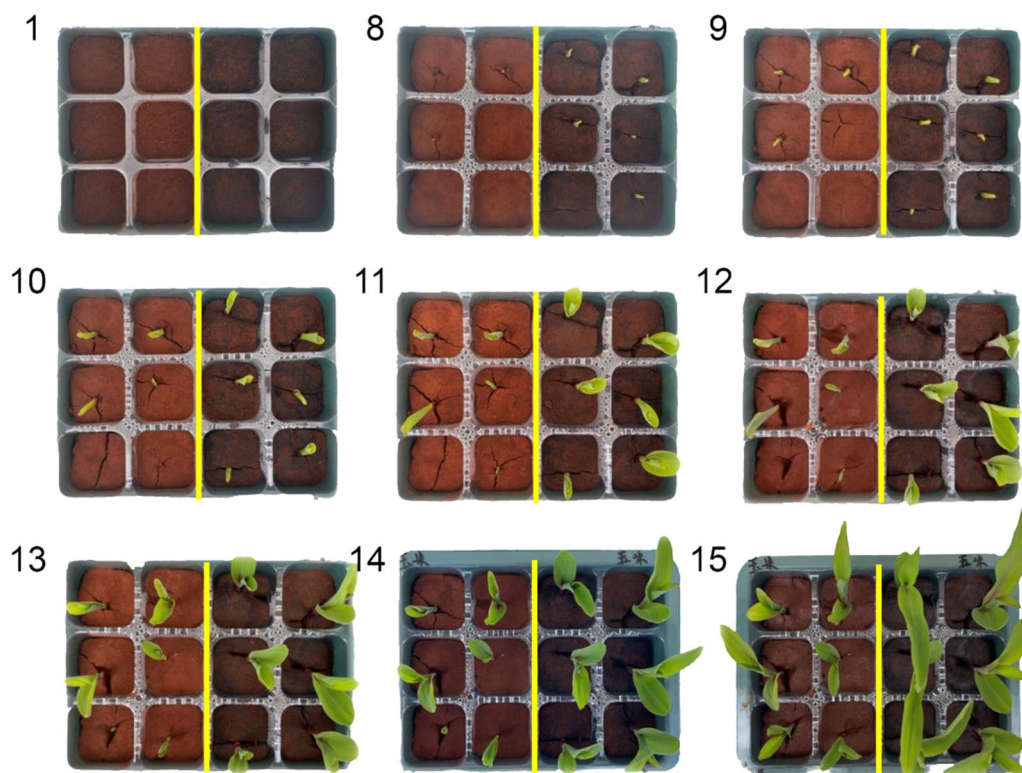

Fig. 8 The growth trend of maize seeds in pure soil sample (two columns on the left) and soil sample mixed with MSBL3 + P (two columns on the right)

plant nutrition can be explored in depth based on this study. On the other hand, since MSBL3 is an adsorbent waste after phosphorus adsorption, backfilling it directly into the soil means that the disposal costs of this waste can be reduced, and therefore, its pricing is slightly negative (Stávková and Maroušek 2021).

3.6 Mechanism discussion

3.6.1 Differences in the crystallinity of La(OH)₃ on the surface of MSB

In the present study, the particle size of the $La(OH)_3$ crystals in MSBL3, MSBL2, and MSBL1 increased in that order, which is related to the amount of $LaCl_3$ input. In general, crystal formation consists of two processes, nucleation formation and nucleation growth, the rates of which are heavily dependent on the reactant concentration. These two processes can be described by Eqs. 1 and 2, where Q is the supersaturation of La^{3+}, s is the equilibrium concentration when La^{3+} is converted to $La(OH)_3$, k is the pre-exponential factor, A is the surface area of the nucleus, D is the diffusion coefficient of the solute La^{3+}, and δ is the distance the nucleus grows in a given direction. When the input of $LaCl_3$ is large, Q of La^{3+} is large, leading to a large v_1. At this point, the process of $La(OH)_3$ nucleation dominates and La^{3+} is consumed at a concentration close to s in a short time, leading to a small v_2 for the subsequent nucleation growth process. As a result, the $La(OH)_3$ crystal particles in the MSBL were highly dispersed and ultrafine at high $LaCl_3$ input (Additional file 1: Fig. S2a). As the amount of $LaCl_3$ input decreases, Q gradually decreases, leading to a decrease in v_1. The decrease in the rate of the nucleation process delays the time required La^{3+} to reach the s state; thus, v_2 increases, resulting in the continuous growth of $La(OH)_3$ crystal nuclei (Additional file 1: Fig. S2b, c). The $La(OH)_3$ crystal size is the largest when the $LaCl_3$ input is the smallest, otherwise, the opposite is true.

$$v_1 = k\frac{(Q-s)}{s} \tag{1}$$

$$v_2 = DA\frac{(Q-s)}{\delta} \tag{2}$$
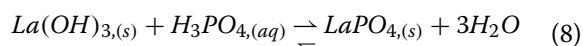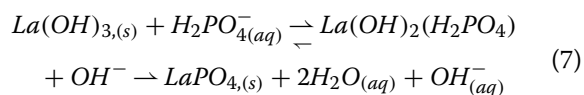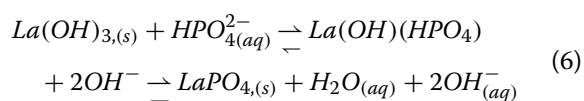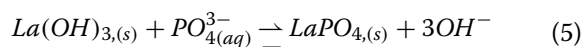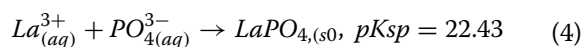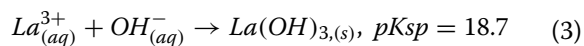
3.6.2 Mechanism of P adsorption by MSBL3

After the adsorption of P by MSBL3, the SEM images showed that the surface of the distorted lamellar structure of MSBL3 was no longer smooth and was replaced by a fluffy spongy layer of the attached material (Additional file 1: Fig. S3 a, b). The elemental mapping (Additional file 1: Fig. S3c–f), and energy-dispersive spectroscopy (Additional file 1: Fig. S3 g) showed that MSBL3 after P adsorption included C, N, O, La, and P,

which were homogeneously distributed, and a new signal peak appeared in the FTIR spectrum (Fig. 1b) of MSBL3, which can be attributed to the P-O bond. In XPS (Fig. 1d), the binding energy of the 3d orbital of La shifted towards a higher binding energy than that before the adsorption of P, but the valence remained at +3. These two phenomena suggest that a new species has been doped into MSBL3, which acts directly on the La^{3+} site. Further direct evidence was provided by PXRD, where the PXRD signal was consistent with that of $LaPO_4$ (JCPDS:35-0731) after P adsorption by MBSL3 (Additional file 1: Fig. S3 h), and the $La(OH)_3$ phase on the MSB carrier was almost completely replaced by the $LaPO_4$ phase.

La^{3+} can form insoluble precipitates $La(OH)_3$ (Eq. 3) and $LaPO_4$ (Eq. 4) with OH^- and PO_4^{3-}, respectively, but $LaPO_4$ had a greater reaction trend with a pKsp as high as 22.43. Thus, $La(OH)_3$ undergoes a complex decomposition reaction with PO_4^{3-} to form $LaPO_4$ (Eq. 4), resulting in the removal of P from water. $H_2PO_4^-$ exists in various hydrolysis forms at different pH, such as H_3PO_4, $H_2PO_4^-$, HPO_4^{2-}, and PO_4^{3-}. When the pH is below 4, it is mainly present as both $H_2PO_4^-$ and H_3PO_4; when the pH is between 4 and 10, it is mainly absent as $H_2PO_4^-$ and HPO_4^{2-}; and when the pH is greater than 10, it is mainly present as HPO_4^{2-} and PO_4^{3-}. At pH 7, P species are present in the form of $H_2PO_4^-$ and HPO_4^{2-}, but PXRD showed that $La(OH)_3$ was converted almost entirely to $LaPO_4$; therefore, the reaction equation for the conversion of $La(OH)_3$ to $LaPO_4$ in a complex decomposition reaction with La species may follow Eqs. 5−8. As seen from Additional file 1: Fig. S1c, when the initial pH of the solution is greater than 4, the pH of the solution after P adsorption by MSBL3 undergoes a certain degree of increase because some or all of the OH^- in $La(OH)_3$ is released in the solution after anion exchange, thus leading to an increase in pH.

The loading of La on MSBL3 was 30.2 wt%, so the theoretical value of 1 g MSBL3 for P adsorption according to $La(OH)_3$ to $LaPO_4$ was 66.91 mg g^{-1}. The experimental results showed that MSBL3 had a capacity of 78.5 mg g^{-1} (at pH3) for P adsorption. Therefore, anion exchange is the main P adsorption pathway. Additionally, there were other interactions. The zeta potential of MSBL3 (Additional file 1: Fig. S1d) showed that the electrostatic potential on the MSBL3 surface was positive when the pH was less than 10.6; therefore, the MSBL3 surface could adsorb P species, such as PO_4^{3-}, HPO_4^{2-}, and $H_2PO_4^-$ via Coulomb interactions. Furthermore, FTIR showed that MSBL3 is rich in N- or O-containing functional groups; therefore, the MSBL3 surface can adsorb P species through hydrogen bonding interactions with PO_4^{3-}, HPO_4^{2-}, $H_2PO_4^-$, and H_3PO_4. Notably, there is no direct

evidence that MSBL3 can adsorb P species by pore-size matching, as this would be difficult to identify in the presence of other driving forces; therefore, this mechanism was not considered. Based on the above discussion, the concept map (Fig. 9) reflects the mechanism of P adsorption by MSBL3 more intuitively.

$$La^{3+}_{(aq)} + OH^-_{(aq)} \rightarrow La(OH)_{3,(s)},\ pKsp = 18.7 \quad (3)$$

$$La^{3+}_{(aq)} + PO^{3-}_{4(aq)} \rightarrow LaPO_{4,(s0},\ pKsp = 22.43 \quad (4)$$

$$La(OH)_{3,(s)} + PO^{3-}_{4(aq)} \rightleftharpoons LaPO_{4,(s)} + 3OH^- \quad (5)$$

$$La(OH)_{3,(s)} + HPO^{2-}_{4(aq)} \rightleftharpoons La(OH)(HPO_4)$$
$$+ 2OH^- \rightleftharpoons LaPO_{4,(s)} + H_2O_{(aq)} + 2OH^-_{(aq)} \quad (6)$$

$$La(OH)_{3,(s)} + H_2PO^-_{4(aq)} \rightleftharpoons La(OH)_2(H_2PO_4)$$
$$+ OH^- \rightleftharpoons LaPO_{4,(s)} + 2H_2O_{(aq)} + OH^-_{(aq)} \quad (7)$$

$$La(OH)_{3,(s)} + H_3PO_{4,(aq)} \rightleftharpoons LaPO_{4,(s)} + 3H_2O \quad (8)$$

4 Conclusions

Currently, the problem of eutrophication in water bodies is serious, and finding suitable adsorbents is the key to applying adsorption methods to avoid eutrophication. In this study, La-based biochar showed good characteristics for the adsorption of P, such as high efficiency, stability, economy, and safety. Among these adsorbents, MSBL3 exhibited the most significant results. The continuous fixed-bed column studied the inhibition of eutrophication, and amplification experiments demonstrated the advantages of MSBL3 in practical engineering applications. It also has good inhibitory properties against *E. coli* and *S. aureus* and can therefore be used to improve water quality. In addition, when MSBL3 reached a fatigued state after P adsorption, it was mixed with a common soil sample to study its effect on the germination and growth of maize seeds. The results showed that it could be used not only as an effective P absorber but also as an
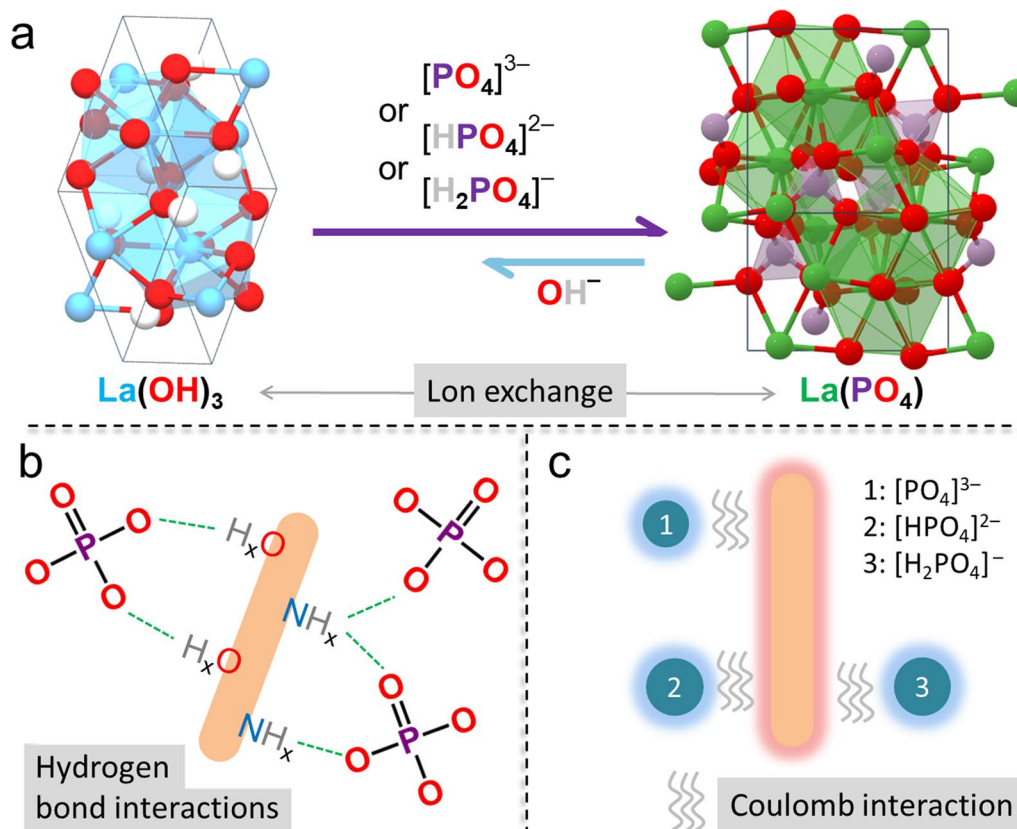

Fig. 9 Adsorption mechanism

effective slow-release P fertilizer. On the other hand, the preparation of 1 g of MSBL3 costs about 1 RMB, and it can reduce the P concentration in 2.6 ton of *Laoyu River* water to below the eutrophication threshold, making this study economically advantageous compared to some process-complex P removal technologies. In conclusion, the La-based biochar prepared in this study is a promising P sorbent for application and is expected to improve the pollution status and the water quality of eutrophic water bodies. Future research will focus on reducing the economic cost and improving the stability of the adsorbent to achieve large-scale application of this technology.

Supplementary Information

The online version contains supplementary material available at https://doi.org/10.1007/s42773-023-00216-y.

Additional file 1: Table S1. List of calculation formulas and models used in this study. **Table S2.** Normality test (pH of solution: 7; Temperature: 298 K; reaction time: 24h). **Table S3.** Parameters of pseudo-first-order and pseudo-second-order kinetic models at different C_0. **Table S4.** Parameters of the Langmuir and Freundlich models and thermodynamics. **Table S5.** Parameters of the Langmuir and Freundlich models and thermodynamics. **Table S6.** Comparison of other adsorbents with MSBL3. **Fig. S1.** Freundlich model. (dosage of adsorbent: 0.5 g/L; T: 298 K). **Fig. S2.** Schematic diagram of the effect of LaCl3 concentration on the size of La(OH)$_3$ crystal formed. The concentration of LaCl$_3$ solute is maximum (a), moderate (b), and minimum (c). **Fig. S3.** (a-b) SEM images of MSBL3 after P adsorption; (c-f) Element mapping of N, O, La, and P of MSBL3+P. EDS (g) and XRD pattern (h) of MSBL3+P. **Fig. S4.** Schematic diagram of fixed-bed column device. **Fig. S5.** Device diagram of magnification experiment.

Declarations

Competing interests
All authors certify that they have no affiliations with or involvement in any organization or entity with any financial interest or non-financial interest in the subject matter or materials discussed in this manuscript.

Author details
[1]Institute for Ecological Research and Pollution Control of Plateau Lakes, School of Ecology and Environmental Science, Yunnan University, Kunming 650504, China. [2]College of Chemistry and Engineering, Yunnan Normal University, Kunming 650092, China. [3]National Engineering Research Center for Marine Aquaculture, Marine Science and Technology College, Zhejiang Ocean University, Zhoushan 316004, China. [4]Key Laboratory of Water and Sediment Sciences, Ministry of Education, College of Environmental Sciences and Engineering, Peking University, Beijing 100871, China. [5]Key Laboratory for City Cluster Environmental Safety and Green Development of the Ministry of Education, School of Ecology, Environment and Resources, Guangdong University of Technology, Guangzhou 510006, China.

References
Agathokleous E, Kitao M, Calabrese EJ (2018) The rare earth element (REE) lanthanum (La) induces hormesis in plants. Environ Pollut 238:1044–1047. https://doi.org/10.1016/j.envpol.2018.02.068

Almanassra IW, McKay G, Kochkodan V, Ali Atieh M, Al-Ansari T (2021) A state of the art review on phosphate removal from water by biochars. Chem Eng J 409:128211. https://doi.org/10.1016/j.cej.2020.128211

Barca C, Gérente C, Meyer D, Chazarenc F, Andrès Y (2012) Phosphate removal from synthetic and real wastewater using steel slags produced in Europe. Water Res 46(7):2376–2384. https://doi.org/10.1016/j.watres.2012.02.012

Bonetta S, Pignata C, Lorenzi E, De Ceglia M, Meucci L, Bonetta S, Gilli G, Carraro E (2016) Detection of pathogenic Campylobacter, E. coli O157:H7 and Salmonella spp. in wastewater by PCR assay. Environ Sci Pollut R 23(15):15302–15309. https://doi.org/10.1007/s11356-016-6682-5

Chen H, Gao Y, Li J, Fang Z, Bolan N, Bhatnagar A, Gao B, Hou D, Wang S, Song H, Yang X, Shaheen SM, Meng J, Chen W, Rinklebe J, Wang H (2022) Engineered biochar for environmental decontamination in aquatic and soil systems: a review. Carbon Res 1(1):4. https://doi.org/10.1007/s44246-022-00005-5

Cordell D, Rosemarin A, Schröder JJ, Smit AL (2011) Towards global phosphorus security: a systems framework for phosphorus recovery and reuse options. Chemosphere 84(6):747–758. https://doi.org/10.1016/j.chemosphere.2011.02.032

Desmidt E, Ghyselbrecht K, Zhang Y, Pinoy L, Van der Bruggen B, Verstraete W, Rabaey K, Meesschaert B (2015) Global phosphorus scarcity and full-scale p-recovery techniques: a review. Criti Rev Env Sci Tec 45(4):336–384. https://doi.org/10.1080/10643389.2013.866531

Durana P, Michalkova L, Privara A, Marousek J, Tumpach M (2021) Does the life cycle affect earnings management and bankruptcy? Oecon Copernic. 12(2):425–461. https://doi.org/10.24136/oc.2021.015

Geng Y-K, Wang Y, Pan X-R, Sheng G-P (2018) Electricity generation and in situ phosphate recovery from enhanced biological phosphorus removal sludge by electrodialysis membrane bioreactor. Bioresour Technol 247:471–476. https://doi.org/10.1016/j.biortech.2017.09.118

Han L, Jing F, Zhang J, Luo X-Z, Zhong Y-L, Wang K, Zang S-H, Teng D-H, Liu Y, Chen J, Yang C, Zhou Y-T (2021) Environment friendly and remarkably efficient photocatalytic hydrogen evolution based on metal organic framework derived hexagonal/cubic In$_2$O$_3$ phase-junction. Appl Catal B-Environ 282:119602. https://doi.org/10.1016/j.apcatb.2020.119602

He J, Wang W, Sun F, Shi W, Qi D, Wang K, Shi R, Cui F, Wang C, Chen X (2015) Highly efficient phosphate scavenger based on well-dispersed La(OH)$_3$ nanorods in polyacrylonitrile nanofibers for nutrient-starvation antibacteria. ACS Nano 9(9):9292–9302. https://doi.org/10.1021/acsnano.5b04236

He Q, Li X, Ren Y (2022) Analysis of the simultaneous adsorption mechanism of ammonium and phosphate on magnesium-modified biochar and the slow release effect of fertiliser. BIOCHAR 4:25. https://doi.org/10.1007/s42773-022-00150-5

Holinger EP, Ross KA, Robertson CE, Stevens MJ, Harris JK, Pace NR (2014) Molecular analysis of point-of-use municipal drinking water microbiology. Water Res 49:225–235. https://doi.org/10.1016/j.watres.2013.11.027

Jia X, Wang H, Li Y, Xu J, Cheng H, Li M, Zhang S, Zhang H, Hu G (2022) Separable lanthanum-based porous PAN nanofiber membrane for effective aqueous phosphate removal. Chem Eng J 433:133538. https://doi.org/10.1016/j.cej.2021.133538

Kumar PS, Korving L, van Loosdrecht MCM, Witkamp G-J (2019) Adsorption as a technology to achieve ultra-low concentrations of phosphate: research gaps and economic analysis. Water Res X. 4:100029. https://doi.org/10.1016/j.wroa.2019.100029

Liu R, Hao X, Chen Q, Li J (2019a) Research advances of Tetrasphaera in enhanced biological phosphorus removal: a review. Water Res 166:115003. https://doi.org/10.1016/j.watres.2019.115003

Liu X, Zong E, Hu W, Song P, Wang J, Liu Q, Ma Z, Fu S (2019b) Lignin-derived porous carbon loaded with La(OH)$_3$ nanorods for highly efficient removal of phosphate. ACS Sustain Chem Eng 7(1):758–768. https://doi.org/10.1021/acssuschemeng.8b04382

Liu Z, Xu Z, Xu L, Buyong F, Chay TC, Li Z, Cai Y, Hu B, Zhu Y, Wang X (2022) Modified biochar: synthesis and mechanism for removal of environmental heavy metals. Carbon Res 1(1):8. https://doi.org/10.1007/s44246-022-00007-3

López-Vázquez CM, Hooijmans CM, Brdjanovic D, Gijzen HJ, van Loosdrecht MCM (2008) Factors affecting the microbial populations at full-scale enhanced biological phosphorus removal (EBPR) wastewater treatment plants in The Netherlands. Water Res 42(10):2349–2360. https://doi.org/10.1016/j.watres.2008.01.001

Maroušek J, Maroušková A (2021) Economic considerations on nutrient utilization in wastewater management. Energies 14:3468. https://doi.org/10.3390/en14123468

Maroušek J, Trakal L (2022) Techno-economic analysis reveals the untapped potential of wood biochar. Chemosphere 291:133000. https://doi.org/10.1016/j.chemosphere.2021.133000

Mayer BK, Gerrity D, Rittmann BE, Reisinger D, Brandt-Williams S (2013) Innovative strategies to achieve low total phosphorus concentrations in high water flows. Crit Rev Env Sci Tec 43(4):409–441. https://doi.org/10.1080/10643389.2011.604262

Sornhiran N, Aramrak S, Prakongkep N, Wisawapipat W (2022) Silicate minerals control the potential uses of phosphorus-laden mineral-engineered biochar as phosphorus fertilizers. BIOCHAR 4:2. https://doi.org/10.1007/s42773-021-00129-8

Stávková J, Maroušek J (2021) Novel sorbent shows promising financial results on P recovery from sludge water. Chemosphere 276:130097. https://doi.org/10.1016/j.chemosphere.2021.130097

Tang Q, Shi C, Shi W, Huang X, Ye Y, Jiang W, Kang J, Liu D, Ren Y, Li D (2019) Preferable phosphate removal by nano-La(III) hydroxides modified mesoporous rice husk biochars: role of the host pore structure and point of zero charge. Sci Total Environ 662:511–520. https://doi.org/10.1016/j.scitotenv.2019.01.159

Tyler G (2004) Rare earth elements in soil and plant systems—a review. Plant Soil 267(1):191–206. https://doi.org/10.1007/s11104-005-4888-2

Wang L, Wang J, Yan W, He C, Shi Y (2020) MgFe$_2$O$_4$-biochar based lanthanum alginate beads for advanced phosphate removal. Chem Eng J 387:123305. https://doi.org/10.1016/j.cej.2019.123305

Wang C, Yu S, Cwiertny DM, Yin Y, Myung NV (2021a) Phosphate removal using surface enriched hematite and tetra-n-butylammonium bromide incorporated polyacrylonitrile composite nanofibers. Sci Total Environ 770:145364. https://doi.org/10.1016/j.scitotenv.2021.145364

Wang X, Li L, Sun F, Wang J, Chang W, Chen F, Peng J (2021b) Detection of mcr-1-positive Escherichia coli in slaughterhouse wastewater collected from Dawen river. Vet Med Sci 7(5):1587–1592. https://doi.org/10.1002/vms3.489

Wei C, Lin WY, Zainal Z, Williams NE, Zhu K, Kruzic AP, Smith RL, Rajeshwar K (1994) Bactericidal activity of TiO$_2$ photocatalyst in aqueous media: toward a solar-assisted water disinfection system. Environ Sci Technol 28(5):934–938. https://doi.org/10.1021/es00054a027

Wu B, Wan J, Zhang Y, Pan B, Lo IMC (2020) Selective phosphate removal from water and wastewater using sorption: process fundamentals and removal mechanisms. Environ Sci Technol 54(1):50–66. https://doi.org/10.1021/acs.est.9b05569

Yang B, Feng Y, Yu Y, He S, Liu H, Xue L, Yang L (2019) Lanthanum ferrite nanoparticles modification onto biochar: derivation from four different methods and high performance for phosphate adsorption. Environ Sci Pollut R 26(21):22010–22020. https://doi.org/10.1007/s11356-019-04553-z

Yao Y, Gao B, Chen J, Yang L (2013) Engineered biochar reclaiming phosphate from aqueous solutions: mechanisms and potential application as a slow-release fertilizer. Environ Sci Technol 47(15):8700–8708. https://doi.org/10.1021/es4012977

Ye Y, Ngo HH, Guo W, Liu Y, Li J, Liu Y, Zhang X, Jia H (2017) Insight into chemical phosphate recovery from municipal wastewater. Sci Total Environ 576:159–171. https://doi.org/10.1016/j.scitotenv.2016.10.078

Yin X, Li X, Petropoulos E, Feng Y, Yang B, Xue L, Yang L, He S (2022) Phosphate removal from actual wastewater via La(OH)$_3$–C$_3$N$_4$ adsorption: performance, mechanisms and applicability. Sci Total Environ 814:152791. https://doi.org/10.1016/j.scitotenv.2021.152791

Yu J, Xiang C, Zhang G, Wang H, Ji Q, Qu J (2019a) Activation of lattice oxygen in LaFe (Oxy)hydroxides for efficient phosphorus removal. Environ Sci Technol 53(15):9073–9080. https://doi.org/10.1021/acs.est.9b01939

Yu S, Li G, Zhao P, Cheng Q, He Q, Ma D, Xue W (2019b) NIR-laser-controlled hydrogen-releasing PdH nanohydride for synergistic hydrogen-photo-thermal antibacterial and wound-healing therapies. Adv Funct Mater 29(50):1905697. https://doi.org/10.1002/adfm.201905697

Zhang X, Wang W, Shi W, He J, Feng H, Xu Y, Cui F, Wang C (2016) Carbon nanofiber matrix with embedded LaCO3OH synchronously captures phosphate and organic carbon to starve bacteria. J Mater Chem A 4(33):12799–12806. https://doi.org/10.1039/C6TA04364J

Zhang W, Qiu X, Wang C, Zhong L, Fu F, Zhu J, Zhang Z, Qin Y, Yang D, Xu CC (2022) Lignin derived carbon materials: current status and future trends. Carbon Res 1:14. https://doi.org/10.1007/s44246-022-00009-1

Zhao Y, Shan X, An Q, Xiao Z, Zhai S (2020) Interfacial integration of zirconium components with amino-modified lignin for selective and efficient phosphate capture. Chem Eng J 398:125561. https://doi.org/10.1016/j.cej.2020.125561